Nucleic Acids Research, 2025, **53**, gkaf1183
https://doi.org/10.1093/nar/gkaf1183
Genomics

Distribution of DNA gyrase cleavage sites across the *Streptococcus pneumoniae* genome: relation to transcription and methylation at GATC sites

María-José Ferrándiz[1], Pablo Hernández[2], Adela G. de la Campa[1,3,*]

[1]Unidad de Genética Bacteriana, Centro Nacional de Microbiología, Instituto de Salud Carlos III, Majadahonda, Madrid 28220, Spain
[2]Departamento de Biología Celular, Centro de Investigaciones Biológicas Margarita Salas, Consejo Superior de Investigaciones Biológicas, Madrid 2804, Spain
[3]Secretaría General, Consejo Superior de Investigaciones Científicas, Madrid 28006, Spain
*To whom correspondence should be addressed. Email: agcampa@isciii.es

Abstract

In bacteria, DNA gyrase plays a key role in cellular processes by affecting supercoiling. However, how gyrase localizes on the chromosome to affect supercoiling is unclear. Here, we interrogate the genome-wide distribution of gyrase in *Streptococcus pneumoniae* by mapping its cleavage sites in the presence of fluoroquinolones. Fluoroquinolones induce the formation of DNA—fluoroquinolone—topoisomerase complexes and generate detrimental double-stranded DNA breaks. Using a chromatin immunoprecipitation-sequencing-based method, we localize gyrase cleavage sites with single-nucleotide resolution. A total of 1517 sites were detected; the majority (92.7%) were located within protein-coding genes and were associated with high-level transcription. This trend was maintained at the level of transcriptional topological domains, where the most transcribed genes exhibited the highest frequency of cleavage sites, while the least transcribed genes exhibited the lowest frequency. We identified a four-base motif, GxxC, in 79% of the sites. The most frequent sequence was GATC (21.2% of all cleavage sites). GATC is the target of three pneumococcal restriction systems: DpnI, DpnII, and DpnIII. We demonstrated that methylation at GATC by the DpnII (GA^{me}TC) or DpnIII (GATC^{me}) systems decreased gyrase cleavage and supercoiling activity. We hypothesized that strains with methylated GATC would be more resistant to subinhibitory concentrations of fluoroquinolones. We indeed demonstrated that gyrase mutants appeared more frequently in strains with GATC methylation (DpnII and DpnIII) than in strains without methylation (DpnI).This is significant for the evolution of fluoroquinolone resistance in *S. pneumoniae*, as the three Dpn phenotypes are present in the population of clinical isolates.

Graphical abstract

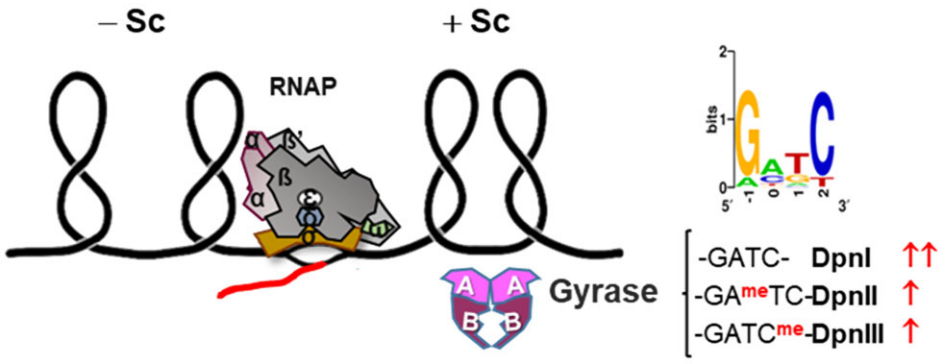

Introduction

Streptococcus pneumoniae is a major human pathogen. It is the most important etiological agent of bacterial community-acquired pneumonia and a main cause of meningitis, bacteremia, and otitis media in children. Pneumococcal diseases remain the leading cause of death among vaccine-preventable diseases worldwide and cause over 1 million deaths annually [1]. The resistance of this bacterium to beta-lactams and macrolides [2] has spread, resulting in the recommendation of fluoroquinolones (FQs) for the treatment of community-acquired pneumonia [3].

Topoisomerases maintain steady-state DNA supercoiling (Sc), which is necessary for replication, transcription, and recombination [4]. FQs target type II topoisomerases,

Received: February 3, 2025. **Revised:** October 9, 2025. **Accepted:** October 11, 2025

topoisomerase IV (Topo IV) and gyrase, which modify Sc by introducing double-stranded transient breaks. In *S. pneumoniae*, FQs target primarily Topo IV [5–8] and secondarily gyrase.

Levofloxacin (LVX) and moxifloxacin (MOX) are the two FQs used clinically for the treatment of pneumococcal diseases. No serious levels of resistance to these drugs in pneumococcus have yet been detected; however, the prevalence of resistance could increase in tandem with an increase in their use [9–11]. FQs induce the formation of DNA–FQ–topoisomerase complexes, which sterically inhibit replication and transcription, and the subsequent generation of detrimental double-stranded DNA (dsDNA) breaks [12]. Bacterial survival depends on the resolution of these breaks. Reactive oxygen species (ROS) contribute to FQ-mediated cell death via a protein-synthesis pathway [13].Treatment of *S. pneumoniae* with LVX or MOX causes double-strand DNA breaks [14–16].

In addition, the transcriptomic response to treatment with these drugs has been related to their lethality. Treatment with LVX at a concentration affecting Topo IV (but not gyrase) triggers a response affecting 5.2% of the genome [17], whereas treatment with MOX at a concentration affecting both Topo IV and gyrase triggers a response affecting 6.5% of the genome [14]. In both cases, the transcriptomic changes triggered by treatment with either drug causes the formation of ROS via the Fenton reaction ($Fe^{2+} + H_2O_2 \rightarrow OH^- + OH^\circ$). These responses are consistent with the general model explaining the lethality of bactericidal antibiotics, which attributes a role to ROS generated via the Fenton reaction (reviewed by [18]). In *S. pneumoniae*, LVX triggers the upregulation of iron uptake genes, and MOX activates pathways leading to the production of pyruvate, which leads to a parallel increase in H_2O_2 mediated by the pyruvate oxidase enzyme SpxB. These ROS contribute to FQ lethality [14, 16, 17].

Sc is tightly regulated. Early evidence comes from the study of *Escherichia coli* deletion mutants lacking Topo I, which showed compensatory mutations in gyrase genes [19,20]. This Sc homeostasis is regulated in bacteria by the transcription of their DNA topoisomerase genes. In *E. coli*, DNA relaxation decreases the transcription of the Topo I gene [21] and increases the transcription of gyrase genes [22, 23]. This is also true in *S. pneumoniae* [24]. Regulation of the transcription of topoisomerase genes (*gyrA* and *gyrB* for gyrase; *parE* and *parC* for Topo IV; and *topA* for Topo I) controls the homeostasis of Sc in *S. pneumoniae* [25]. This regulation is part of a global transcriptomic response to changes in Sc, which has been detected both under DNA relaxation by treatment with the gyrase inhibitor novobiocin [26, 27] and under hyper-Sc induced by the inhibition of Topo I by seconeolitsine [28]. These Sc changes triggered coordinated transcriptional regulation of genes clustered in domains. Moderate DNA relaxation induced by the inhibition of gyrase with novobiocin, i.e. a decrease in Sc density (σ) of ∼40%, modulates the transcription of 37% of the genome with a majority (>68%) of responsive genes clustered in 15 upregulated (UP) or downregulated (DOWN) domains [26]. Greater relaxation induced by increased TopoI expression, i.e. a decrease in σ of 90%, induces broader domains, which include 52% of the genome [27]. On the other hand, hypernegative-Sc (an increase in σ of 70%) modulates the transcription of 10% of the genome, with 25% of responsive genes grouped into 12 Sc domains [28].

There are other types of gene domains that do not respond to Sc changes [29], such as pcNR (position-conserved nonregulated) and AT-rich (ATr) domains. The AT content is greater in the UP domains than in the DOWN domains. The UP, DOWN, and pcNR domains are enriched in essential genes and those of the central metabolic network, whereas ATr genes have the lowest transcription levels and may play a structural role [30]. The location of Sc domains is conserved in the *Streptococcus* genus [25], suggesting topology-driven evolution. The location of topoisomerase genes in the Sc domain determines their transcriptional regulation [25]: *topA* is located in a DOWN domain and *gyrB* is located in an UP domain.

In this way, Sc regulates transcription, and transcription is, at the same time, a major contributor to the level of Sc. The first observation in this regard was that the transcription of a plasmid-encoded gene affected Sc levels when Topo I mutants were used [31]; this fits into the twin Sc-domain model, which proposes that domains of negative and positive Sc are transiently generated behind and ahead of the moving RNA polymerase, respectively [32]. *In vitro* studies support both this model and a role for Topo I in removing R-loops, which would otherwise interfere with transcription elongation [33–35]. In addition, physical interactions between Topo I and RNA polymerase have been detected *in vitro* in *E. coli* [36] and *S. pneumoniae* [37]. Furthermore, ChIP-seq experiments have shown *in vivo* colocalization of RNA polymerase, Topo I, and gyrase on the active transcriptional units of *Mycobacterium tuberculosis* [38], and genome-wide proximity between Topo I and RNA polymerase in *S. pneumoniae* [37] and *E. coli* [39], supporting the interplay between transcription and Sc.

Although *in vitro* mapping of the pneumococcal Topo IV and gyrase cleavage sites (GCSs) has been performed [40, 41], a genome-wide approach has not been used. The aim of the present study was to map gyrase binding sites genome-wide in an attempt to understand the role of this enzyme in organizing the genome into transcriptional domains, including Sc-dependent (UP and DOWN) and Sc-independent (pcNR and ATr) domains. Since our attempts to localize gyrase binding sites via Chip-seq were unsuccessful, we used the single-nucleotide resolution method described to map *E. coli* GCSs across the genome in FQ-treated samples [42]. Using this method, we were able to map GCSs in the *S. pneumoniae* genome in cultures treated with two clinically used FQs, LVX, and MOX. To perform ChIP experiments, a strain containing the GyrA protein tagged at the C-terminus with 3 × Flag was constructed, and anti-Flag antibodies were used. These experiments have permitted the mapping of GCSs in the genome and the determination of the role of gyrase in transcription in *S. pneumoniae*, as well as its preferential location in transcriptional domains.

Materials and methods

Microbiological methods and genetic constructions

Streptococcus pneumoniae R6 and T1 (as R6, ParCS79F) [43] strains were grown at 37°C in casein hydrolysate-based liquid medium (AGCH) supplemented with 0.2% yeast extract and 0.3% sucrose (A + Y) and transformed as described previously [44]. The minimum inhibitory concentrations (MICs) for R6 and T1 were 0.25 and 2 μg/ml for LVX, respectively, and 0.125 μg/ml for MOX.

An R6-derived strain containing the GyrA subunit of gyrase tagged with 3 × Flag at the C-terminus (R6GA3F) was constructed by replacing the *gyrA* wild-type allele with *gyrA*3 × Flag. For that purpose, three DNA fragments were obtained via polymerase chain reaction (PCR) with the primers detailed in Supplementary Table S1, ligated, and used to transform *S. pneumoniae*. The first PCR product (2996 bp) included *gyrA* with the sequence encoding the 3 × Flag peptide fused to its 3′ end. It was amplified from the R6 chromosome via the primers GYRAPROM2 and GYRA3FLAGXBA (containing the sequence for 3 × Flag followed by an XbaI restriction site). The second product (1078 bp), which contained the chloramphenicol resistance cassette (*cat*), was amplified from the pJS3 plasmid with the primers UPPTETXBA and CATDOWNSALTER, which contained XbaI and SalI restriction sites, respectively. The third fragment (1582 bp), containing the genes *srtA* and *nirC* (downstream of *gyrA*), was amplified from R6 with the primers SRTA184SAL and SPR1095R1, the former carrying a SalI restriction site. These three PCR products were digested with the corresponding restriction enzymes and ligated. The ligation product was used as a template to obtain a 5395 bp PCR product with the oligonucleotide pair GYRAPROM2/SPR1095R1, which was subsequently used to transform R6 competent cells. Transformants were selected by plating on A + Y agar medium supplemented with 2.5 μg/ml chloramphenicol. The replacement of *gyrA* with *gyrA*3 × Flag was confirmed by amplification of the chromosome with the primers GYRAPROM1 and SPR1095R2, which flanked the inserted DNA, and by sequencing *gyrA*3 × Flag with the primers GYRAPROM1, GYRA44, GYRA8, GYRA430, and CAT9.

To construct T1-derivative strains encoding diverse Dpn systems, the following procedure was followed. First, the *dpnCD* operon was replaced by the erythromycin resistance determinant *ermB* in strain T1. For this purpose, *ermB* was amplified via PCR from the plasmid pJDC9 with the primers ERMECO and ERMHIN, yielding a 992 bp fragment. Two more fragments flanking upstream and downstream of *dpnCD* were amplified by PCR from the R6 chromosome with primer pairs GALTF1/SPR1666R1ECO (846 bp) and PBUXF1HIN/PBUXR1 (972 bp), respectively, with the former containing an EcoRI site and the latter containing a HindIII site. The fragments were digested and ligated. The resulting ligation products were amplified via PCR with the primer pair GALTF1/PBUXR1, yielding a 3953 bp PCR fragment, which was subsequently used to transform competent T1 cells. Recombinant colonies were selected by plating on A + Y agar medium supplemented with 2 μg/ ml of erythromycin. To check for the deletion of *dpnCD*, the DNA of resistant colonies was amplified with the primers GALTF2/PBUXR2, which encompass the exchanged fragment. The resulting strain named T1ΔDpn was used to construct a series of derivative strains carrying either the DpnI (*dpnCD*), DpnII (*dpnABC*) or DpnIII (*m.dpnIII*, *r.dpnIII*) restriction enzyme systems, all of which carry promoters and transcription termination signals. These cassettes were amplified via PCR from strains R6 (DpnI), HB264 (DpnII) [45], and ATCC700669 (DpnIII [46] and introduced into the *spr1865* locus via recombination. Three DNA fragments were obtained via PCR. The first product (1537 bp), containing the kanamycin resistance determinant and *spr1864*, was amplified from the R6 P_{Zn}*topA* chromosome [27] using the primers KANRSAC (containing a SacI restriction site) and SPR1863F. The second product contained DpnI (1614 bp), DpnII (2851 bp), or DpnIII (3078 bp) via the primers DPNUPSAC with either DPNR6DOWNSAL, DPN23FDOWNSAL, or DPNHBDOWNSAL. These primer pairs contain restriction sites for SacI and SalI. The third fragment (671 bp) contained the *spr1866* gene and was amplified from the R6 P_{Zn}*topA* chromosome with the primers TERSAL (containing a SalI restriction site) and SPR1866R. These three PCR products were digested and ligated. Ligation products were used as templates to obtain PCR products of 3822 bp (DpnI), 5 286 bp (DpnII), and 5 059 bp (DpnIII) with the oligonucleotide pair SPR1863F/SPR1866R. These fragments were used to transform R6GA3FΔDpn and T1ΔDpnpLS1 competent cells, and the transformants were selected with 0.25 mg/ml kanamycin. To confirm the insertion of the *dpn* operons, amplification from the chromosome was performed with the primers SPR1863F2 and SPR1866R2 flanking the inserted DNA. The resulting strains were named T1ΔDpn + DpnI, T1ΔDpn + DpnII, and T1ΔDpn + DpnIII.

Analysis of chromosomal fragmentation

Chromosomal fragmentation was detected by pulse-field gel electrophoresis (PFGE) as previously described [14]. Approximately 3 × 10^6 cells were included in agarose plugs, lysed, and treated with proteinase K. Plugs were placed into the wells of a 1% low-gelling agarose (Bio-Rad) gel in 0.5× TBE buffer [45 mM Tris-borate, pH 8.0, 1 mM ethylenediaminetetraacetic acid (EDTA)]. The gels were electrophoresed at 14°C in a Cheff-DR III System (Bio-Rad), during 22 h at 5.8 V/cm with a 0.1–40 s switch-time ramp. The samples were stained with 0.5 μg/ml ethidium bromide. Chromosomal fragmentation was estimated by quantifying the band intensities of the fragments (compression zone, CZ) versus the whole signal in the lane using Image Lab software (BioRad).

Gyrase purification and *in vitro* assays

Gyrase was purified as previously described [47]. The GyrA and GyrB proteins were hyperproduced via the pQE1 vector/M15(pREP4) system, which permits the controlled hyperproduction of proteins with an N-terminal M-K-(H)6-Q fusion encoded by genes placed under the control of a T5 promoter and two *lac* operator sequences. The pREP4 plasmid constitutively expresses the LacI repressor. The expression of recombinant proteins, which genes were cloned into pQE vectors, was induced by isopropyl-β-d-thiogalactopyranoside, which binds to LacI and inactivates it. This inactivation allows the host cell's RNA polymerase to transcribe sequences downstream from the T5 promoter. Gyrase Sc activity was determined as described previously [47] using pLS1 plasmids obtained from strains harboring the DpnI, DpnII or DpnII system. MOX-mediated gyrase cleavage was performed with a reconstituted enzyme using a 1:4 ratio of GyrA:GyrB incubated for 1 h at 4°C. Cleavage assays were carried out in 35 mM Tris–HCl (pH 7.5), 24 mM KCl, 4 mM $MgCl_2$, and 2 mM Ditiotreitol as described previously [47]. The reconstituted enzyme (400 ng of GyrA:1600 ng of GyrB) was incubated with 0.4 μg of the CCC pLS1 plasmid in 20-μl reaction mixtures in the presence of MOX. After a 15 min incubation at 37°C, 1 μl of 10% sodium dodecyl sulfate (SDS) and 2 μl of 20 mg/ml proteinase K were added, and the mixture was incubated for 30 min at 45°C. The samples were analyzed via electrophoresis in 1% agarose gels, which were run at 2 V/cm for 12 h. The gels were stained with 0.5 μg/ ml ethidium bromide and photographed

under UV light. Cleavage activity was estimated by quantifying the band intensities of the plasmid in its linear form (L) versus the total plasmid signal (CCC + L + OC) using Image Lab software (BioRad).

Two-dimensional agarose gel electrophoresis

The isolation of pLS1 plasmid DNA from *S. pneumoniae* cultures grown on A + Y medium supplemented with 1 μg/ml tetracycline was performed via a neutral method that avoids plasmid denaturation [48]. Exponentially growing cells were harvested and lysed by treatment with lysozyme and a detergent solution (1% Brij 58, 0.4% sodium deoxycholate). Plasmid topoisomers were analyzed in neutral/neutral two-dimensional agarose gels. The first dimension was run in a 0.4% agarose (Seakem; FMC Bioproducts) gel in 1 × Tris-borate-EDTA (TBE) buffer containing 1 μg/ml of chloroquine (Sigma) at 1.5 V/cm at room temperature for 19 h. The second dimension was run in a 1% agarose gel in TBE containing 2 μg/ml of chloroquine at 7.5 V/cm for 7–9 h at 4°C. Chloroquine was added to the TBE buffer in both the agarose and running buffers. After electrophoresis, the gels were subjected to Southern hybridization using a 240 bp PCR fragment obtained from pLS1 DNA with 5′-biotinylated pLS1F and pLS1R (Supplementary Table) as the probe on gels transferred to nylon membranes (Inmobylon NY+; Millipore). Chemiluminescent detection of DNA was performed with a Phototope-Star kit (New England BioLabs). Images were captured with a VersaDoc MP400 system and analyzed with the Quantity One program (Bio-Rad). The DNA linking number (Lk = Tw + Wr) was estimated by quantifying the amount of each topoisomer. The DNA Sc density (σ) was calculated using the equation $\sigma = \Delta Lk/Lk_0$. Changes in the linking number (ΔLk) were determined using the equation $Lk = Lk - Lk_0$, in which $Lk_0 = N/10.5$, N is the length of the DNA in bp (4408 bp for pLS1), and 10.5 is the number of bp per complete turn in B-DNA, the most likely helical repeat of DNA under the conditions used. To simplify, σ = Lk of the most abundant topoisomer/(N/10.5). The most abundant topoisomer was identified by densitometry, and its Lk was calculated considering that the topoisomer that migrates with ΔLk = 0 in the second dimension has ΔWr = −14 (pLS1), given the positive supercoils introduced by 2 μg/ml chloroquine.

Immunoprecipitation and construction of sequencing libraries for the identification of GCSs

Mapping of the GCSs was achieved following the Topo-Seq method essentially as described previously [42]. This ChIP-seq-based method takes advantage of the ability of topoisomerase poisons, such as LVX and MOX, to stabilize the cleaved DNA–gyrase complex, where gyrase remains covalently linked to the 5′ ends. In this way, the 5′ ends are not ligated to adapters; therefore, the corresponding strands are not present in the sequencing library. The only DNA chains that are sequenced are those whose 3′-ends are oriented toward the gyrase cutting sites, where adapters are ligated. Mapping these 3′ ends allows GCSs to be localized genome-wide with single-nucleotide resolution.

Cultures of 80 ml of strain R6GA3F were grown to OD_{620nm} = 0.4 and treated for 15 min with LVX or MOX at concentrations equivalent to 512× MIC to trap covalent gyrase–DNA cleavage complexes. Parallel cultures of the same strain grown under the same conditions were left untreated (NT control). The cells were washed with phosphate-buffered saline three times and suspended in buffer 1 (50 mM HEPES-KOH, pH 7.55; 140 mM NaCl; 1 mM EDTA; 1% Triton X-100; 0.1% sodium deoxycholate; 1 mM Phenylmethylsulfonyl fluoride; 0.1 mg/ml RNase A). Cellular lysis and DNA shearing were performed by applying 18–30 cycles (30 s ON/ 30 s OFF) of ultrasound with a Bioruptor (Diagenode) in 0.1 ml tubes. The sheared DNA ranged from 200 to 700 bp in size. A portion of the lysate (~5×10^8 cells) was retained as a mock control fraction (−IP). The rest of the lysate was immunoprecipitated (+IP) with 10 μg of anti-Flag antibody (Invitrogen), directed against GyrA-3 × Flag, coupled to 100 μl of protein G Dynabeads (Invitrogen) for 4 h at 4°C. The immunoprecipitated complexes were washed once with 1 ml of buffer 1 without RNase A; once with buffer 1 with 500 mM NaCl instead of 140 mM NaCl; and once with buffer 2 (10 mM Tris–HCl, pH 8, 250 mM LiCl, 1 mM EDTA, 0.5% NP40, 0.5% sodium deoxycholate). The complexes were diluted in 500 μl of TES buffer (10 mM Tris–HCl, pH 8; 250 mM NaCl; 1 mM EDTA) containing 0.5 mg/ml proteinase K and incubated overnight at 65°C. Immunoprecipitated DNA was extracted with phenol:chloroform:isoamyl alcohol (25:24:1), precipitated with ethanol and resuspended in 25 μl of H_2O. Two biological replicates were performed for each antibiotic used. As a result of the procedure described, the following samples of immunoprecipitated DNA were obtained: replicates 1 and 2 of samples treated with MOX (MOX1, MOX2), replicates 1 and 2 of samples treated with LVX (LVX1, LVX2) and replicates 1 and 2 of untreated samples (NT1, NT2). DNA libraries were generated via the Accel NGS 1S Kit (Swift Bioscience) following the manufacturer's instructions, and sequencing was performed on the Illumina NovaSeq platform applying a single-strand paired-end sequencing protocol. The immunoprecipitated DNA from MOX and LVX treated cultures was enriched in gyrase cleavage fragments. The 5′ ends of these cleavage sites were blocked by a peptide from GyrA, even after proteinase K treatment, and therefore they were refractory to adapter ligation. Consequently, the only DNA chains sequenced were those whose 3′ ends were oriented toward the GCS [42].

Analysis of sequencing data and gyrase cleavage site calling

Analysis of sequencing reads was carried out using the web-based platform Galaxy [49]. The quality of the raw sequence data was analyzed with the FASQC tool. The reads were mapped against the *S. pneumoniae* R6 genome (ASM704v1) using the BWA-MEM2 software package in simple analysis mode. The resulting BAM files were used as inputs in the BamCoverage tool to obtain coverage tracks of the aligned sequences at the single nucleotide level (Bin = 1), which were normalized to the total number of reads mapped in each experiment. The BamCoverage tool was also used to determine the genome-wide coverage of the 3′ ends and 5′ ends of the aligned reads. Thus, for each position in the genome, we obtained the number of 3′ ends and 5′ ends that mapped at that position and the number of reads that overlapped. Integrative genomics viewer (IGV) was used for visualization of coverage.

GCSs are characterized by a low-coverage 4 bp gap that corresponds to the cleaved sequence (positions n2 to n5), flanked

by a highly enriched nucleotide on either side of the gap (positions n1 and n6), corresponding to the 3′ ends of the reads obtained with the Topo-Seq method [42]. To identify the cleavage sites generated by stabilization of the gyrase–DNA cleavage complexes with FQs, the genome-wide coverage of 3′-ends in treated and untreated cells was compared using the Audic-Claverie statistical test [42]. Only positions significantly enriched upon treatment in 3′-ends with a *P*-value of .005 were considered candidates for positions n1 and n6. The cleavage sites were finally called if, among these candidates, the values of 3′-end coverage met the following requirements: counts at the n1 and n6 positions must be at least four times greater than the average values at positions n2 through n5.

Results

Locations of gyrase cleavage sites in the genome

We used the Topo-Seq method [42], a ChIP-seq-based method that takes advantage of the ability of FQs to stabilize the cleaved DNA–gyrase complex, where gyrase remains covalently linked to the 5′ ends. Gyrase generates 4 bp 5′-terminal extensions. In this method, the 5′ ends are not ligated to adapters; therefore, the corresponding strands are not present in the sequencing library. The only DNA chains that are sequenced are those whose 3′ ends are oriented toward the gyrase cutting sites, where adapters are ligated. Mapping these 3′ ends allows GCSs to be localized genome-wide with single-nucleotide resolution (Fig. 1).

To facilitate immunoprecipitation, we constructed the R6GA3F strain, in which GyrA was tagged at its C-terminus with a 3 × Flag peptide. To allow optimal growth conditions, we used exponentially growing cultures (grown to OD_{620nm} = 0.4) that were treated for a short time (15 min) with concentrations equivalent to 512× MIC of LVX or MOX to trap covalent gyrase−DNA cleavage complexes. We used equivalent drug concentrations (in terms of the fold of the MIC) as those previously used by Sutormin *et al.* [42]. These concentrations were saturating since no significant increase in CZ *in vivo* cleavage was observed when comparing diverse concentrations (10×, 100×, 250×, and 500× MIC) of the drugs (see Supplementary Fig. 1). At these concentrations, many cleavage sites were detected. A culture grown under the same conditions but without any treatment (NT control) was grown simultaneously. Anti-Flag antibodies were used for immunoprecipitation. These experiments were performed in duplicate. A total of 1663 and 1853 GCSs were detected in the LVX-treated cultures, with the majority of sites being common to both experiments (Fig. 2A). In the cultures treated with MOX, the number of GCSs differed between the two experiments, with one showing approximately four times the number of sites (3986) than the other (1009 sites), although 903 sites were common to both experiments (Fig. 2B). Based on these data, the 1517 cleavage sites common to both treatments (1 + 2 with LVX and 1 + 2 with MOX) (Fig. 2C) were considered for further analysis. The same GCS motif was identified when MOX, LVX, or MOX + LVX were analyzed separately (Fig. 2C).

Mapping of these sites in the genome is shown in Fig. 3. Among these 1517 GCSs, 1406 were located in protein-coding genes, 54 in the four ribosomal RNA (rRNA) operons (Figs 3 and 4), and 57 in extragenic positions. A high concentration of GCSs downstream of the rRNA operons was evident (Fig. 4).

GCSs are associated with transcription and genes encoded in DOWN and pcNR domains

The presence of GCSs was associated with high transcription. We used the RPKM (reads per kilobase per million mapped reads) from our RNA-seq experiments of exponentially growing cultures grown under the same conditions [28] to classify genes as highly expressed (HE) or expressed at low levels (LE). When the presence of GCSs in the 250 more HE genes was compared with that in the 250 fewer LE genes, a significant difference was observed, both between the HE and LE genes and between the LE genes and all genes (in both cases P = .0002) (Fig. 5A).

The presence of GCSs was also analyzed across genes (Fig. 5B): upstream (A), 5′-end (B), 3′-end (C), and downstream (D). GCSs were significantly more common in the gene, as shown by the different frequency between A and B ($P = 6.15 \times 10^{-6}$) and between C and D ($P = 9.12 \times 10^{-7}$).

When the transcriptional topological domains detected under DNA relaxation by the inhibition of gyrase with novobiocin [26] were considered, the DOWN and pcNR domains presented the highest frequency of GCSs, whereas ATrs presented the lowest frequency (Fig. 5C). Compared with the UP domains, the DOWN domains presented the highest number of GCSs ($P = 4 \times 10^{-4}$) and ATr domains (4.1×10^{-7}). In addition, a significant difference was also observed between pcNR and UP ($P = 1.7 \times 10^{-3}$) and between pcNR and ATrs ($P = 7.7 \times 10^{-6}$).

These results suggest that GCS locations are associated with gene transcription (Figs. 5A and B). The DOWN and pcNR domains exhibited high transcription efficiency and a high presence of GCSs. In contrast, the UP domains showed a low presence of GCSs and the ATr domains showed an almost complete absence of GCGs (Fig. 5C).

Consensus GCS

The same four-base GCS motif was identified regardless of the FQ used (Fig. 2). There are 69 867 GxxC sequences in the genome, 3567 of which correspond to GATC (5.11%). Among the 1517 GCSs detected, 1198 (79%) are GxxC, and 321 (26.8%) have the GATC sequence. Although GATC is not the most abundant GxxC sequence in the genome, it is the most frequently cleaved sequence by gyrase, accounting for 21.1% of the cleavage sites (Fig. 6).

Other sequence features are also involved in sequence recognition by gyrase. The alignment of the sequences flanking the GCSs indicated a potential motif (Fig. 7). A symmetrical pattern was observed at both sides of the cleavage site with a phased 10-bp GC content. This pattern was partially detected in the GATC sequences that were cleaved, but not when all GATC sequences were considered.

Methylation of GATC sequences affects fragmentation and Sc

We hypothesize that methylation of GATC could interfere with gyrase cleavage. *S. pneumoniae* possesses three restriction–modification systems that act on this sequence, DpnI, DpnII, and DpnIII (Fig. 8A). DpnI (*dpnCD*) codes for the DpnI (*dpnC*) restriction enzyme that cuts dsDNA that is methylated on the A base of GATC [51]. The DpnII (*dpnABC*) system codes two methylases, which methylate the A base of GATC on either dsDNA (DpnM) or single-stranded DNA (DpnA) and a restriction enzyme (DpnII,

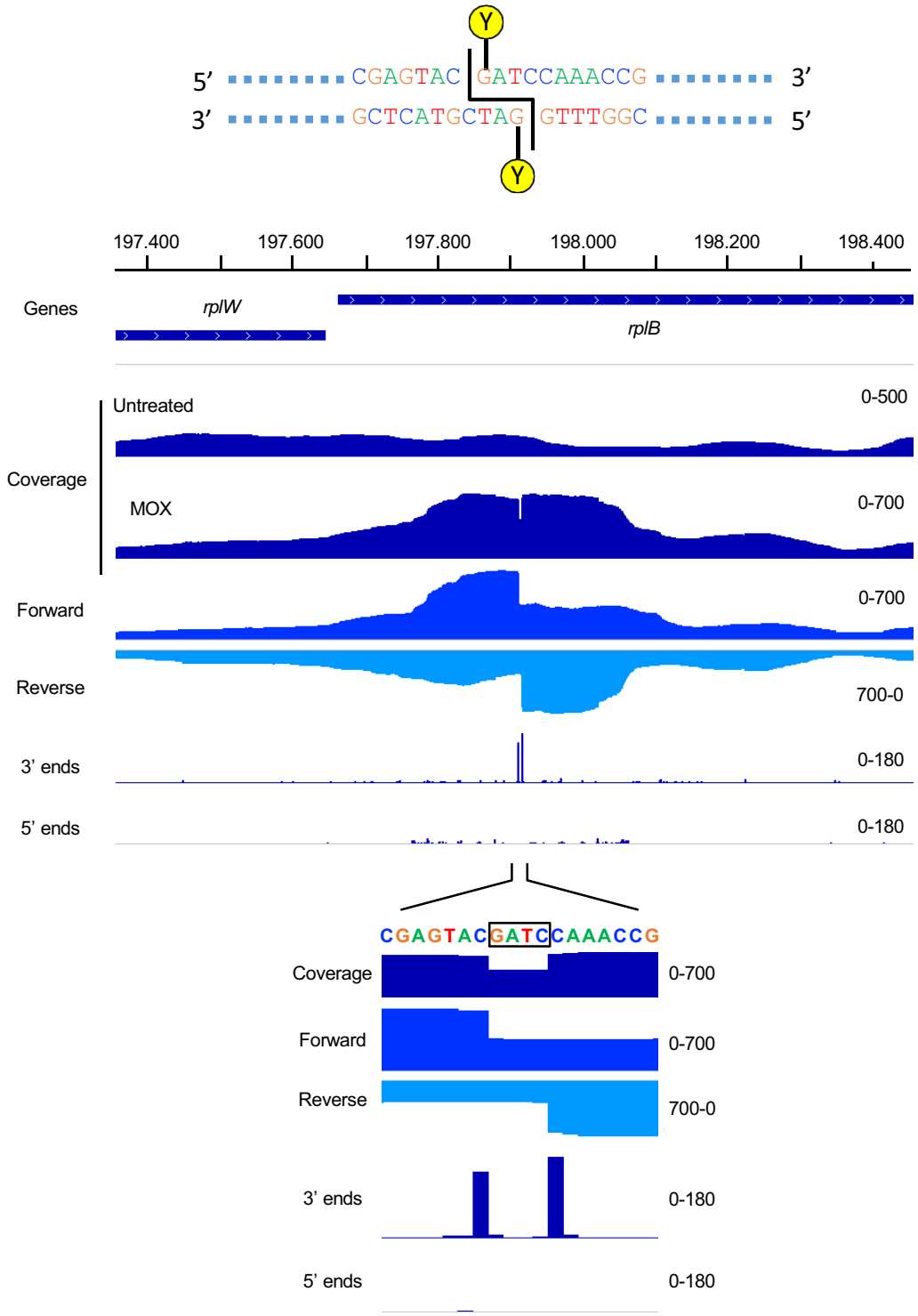

Figure 1. Mapping of GCSs via the Top-Seq method. The results are shown for cleavage at the GATC site at *rplB* in the presence of MOX, as visualized in IGV. At the top is a representation of the double-stranded sequence cleaved by gyrase. The 5′ends are blocked by peptides, including the catalytic Tyr (**Y**), which is shown in yellow. The total sequencing coverage depth is shown in dark blue (both untreated and MOX-treated samples). Coverage depth for forward and reverse strands is shown in light blue and turquoise, respectively.

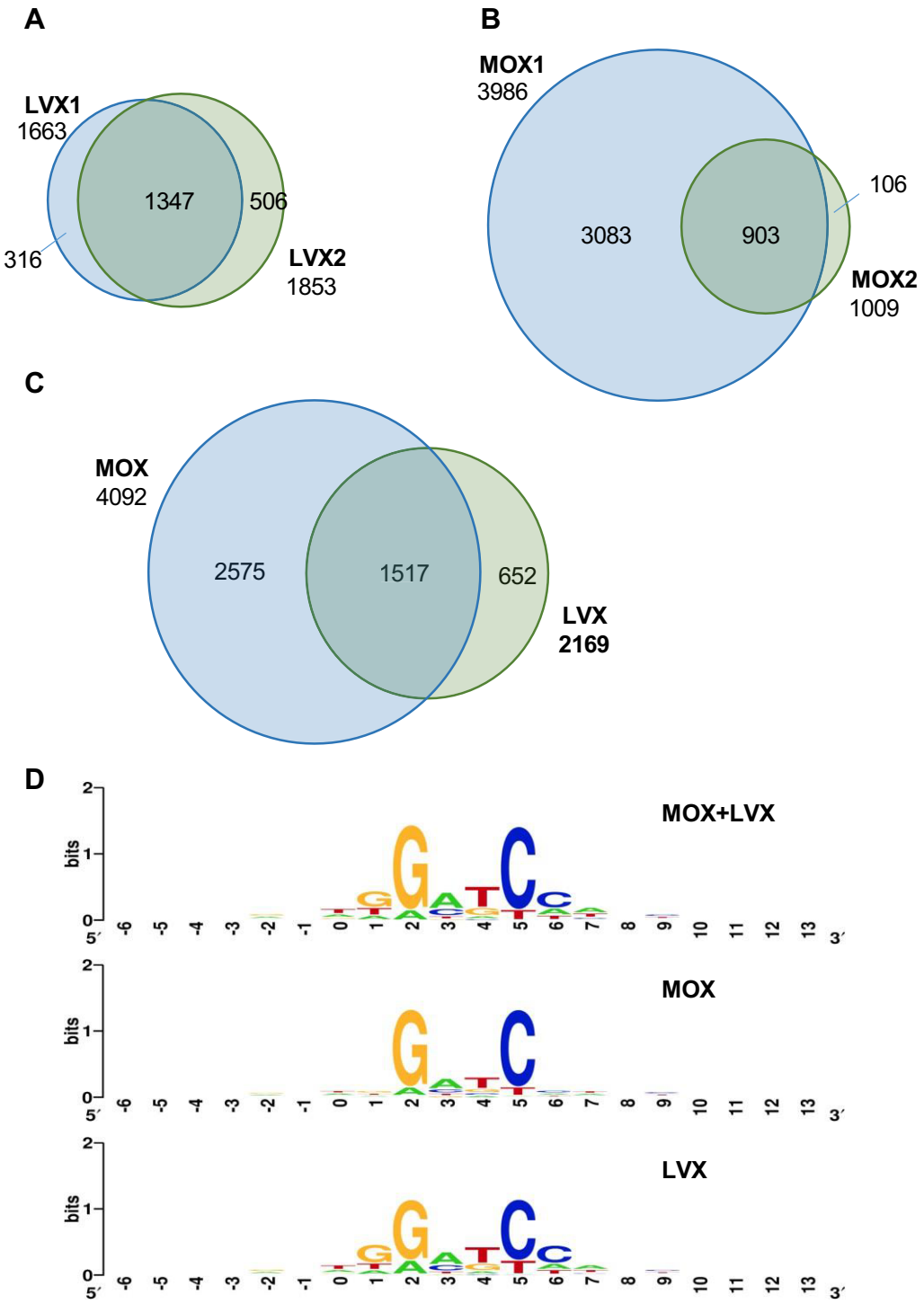

Figure 2. Venn diagram representations indicating GCSs identified in cultures treated with LVX. (**A**), MOX (**B**) or both MOX and LVX (**C**). (**D**) Logos of the gyrase cleavage sequences in the MOX, LVX, or MOX + LVX treatment groups. LVX1 and LVX2 denote results of two independent replicates. The same apply to MOX1 and MOX2.

encoded by *dpnB*) that cuts nonmethylated GATC [52–54]. Another system, DpnIII (*m.dpnIII*, *r.dpnIII*), present in one of the main multidrug-resistant clones, Spain^{23F}-ST81. This system codes for a methylase of the C base of GATC on ds-DNA and a restriction enzyme that cut nonmethylated GATC [46]. We constructed three strains to analyze the role of GATC methylation in gyrase cleavage. To study the cleavage induced by gyrase in the presence of FQs, we chose strain T1, an R6 derivative strain that carries a ParCS79F change [43], which makesTopo IV resistant to low LVX concentrations, i.e. lower than or equal to 10 × MIC, [43]. First, the *dpnCD* genes of T1 were deleted and the genes coding for the three restriction systems were introduced ectopically at *spr1865* (Fig. 8A).

We quantified chromosomal fragmentation after LVX or MOX treatment via PFGE. The CZ, the band that contains the large-size nicked chromosomal DNA fragments that re-

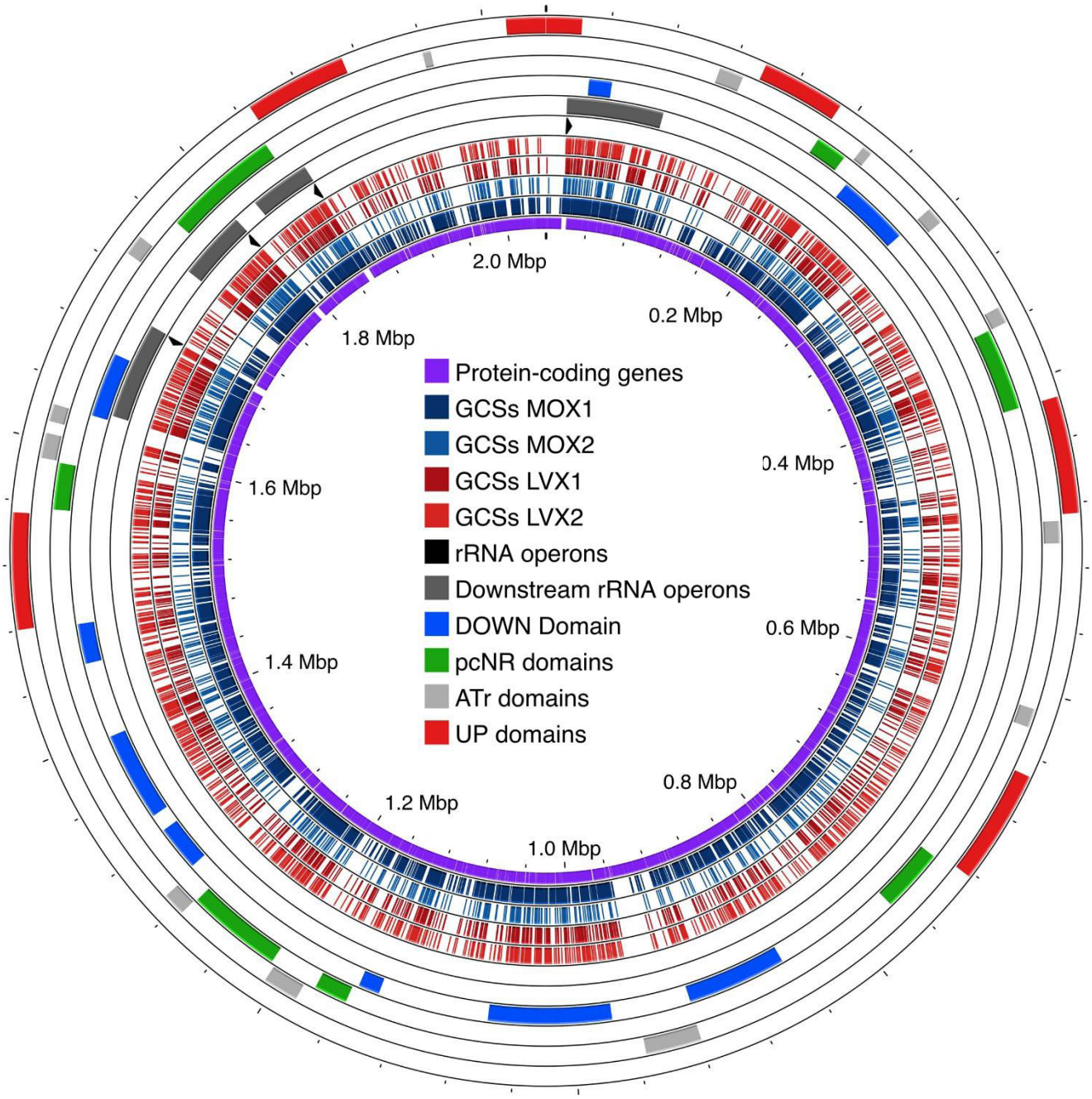

Figure 3. Mapping of the GCSs found under the different treatments and cultures. The transcriptional domains previously characterized in the pneumococcal genome [29](UP, DOWN, pcNR, and ATrs) are indicated, as are the rRNA operons (black arrowheads). The map was generated with the Proksee program [50].

main unresolved in the gel, was used to estimate fragmentation [14]. At the LVX concentration used (10 × MIC, 5 μg/ml) only gyrase is inhibited. However, at the concentrations used in the MOX treatments, both gyrase and Topo IV were inhibited. As shown in Fig. 8 fragmentation increased under FQ treatment. In the presence of LVX (Fig. 8B and C), the greatest degree of fragmentation was observed in the strain carrying DpnI genes (nonmethlylated GATC), followed by the strain carrying DpnII ($GA^{me}TC$) and that carrying DpnIII ($GATC^{me}$). The amount of CZ generated in the presence of 10 × LVX in relation to the untreated cultures was 3.10 ± 0.52, 1.58 ± 0.37, and 1.51 ± 0.15 for the DpnI, DpnII, and DpnIII strains, respectively (mean ± SD, $n = 3$).

Comparison of the amount of CZ generated in the presence of 10 × MOX in relation to the untreated cultures revealed values (mean ± SD, $n = 3$–6) of 1.47 ± 0.31, 1.17 ± 0.29, and 1.00 ± 0.15 for the DpnI, DpnII, and DpnIII strains, respectively. For 100 × MIC, those values were 2.27 ± 0.31, 1.17 ± 0.49, and 1.00 ± 0.16, respectively. These results revealed lower cleavage in the DpnIII strain than in the other two strains in the presence of high MOX concentrations. While differences between the DpnI and DpnII strains were detected in the presence of 10 × the MIC of LVX (Fig. 8B and C), these differences were not detected in the presence of MOX (Fig. 8D and E), although differences were detected between the DpnII and DpnIII strains in the presence of MOX. The

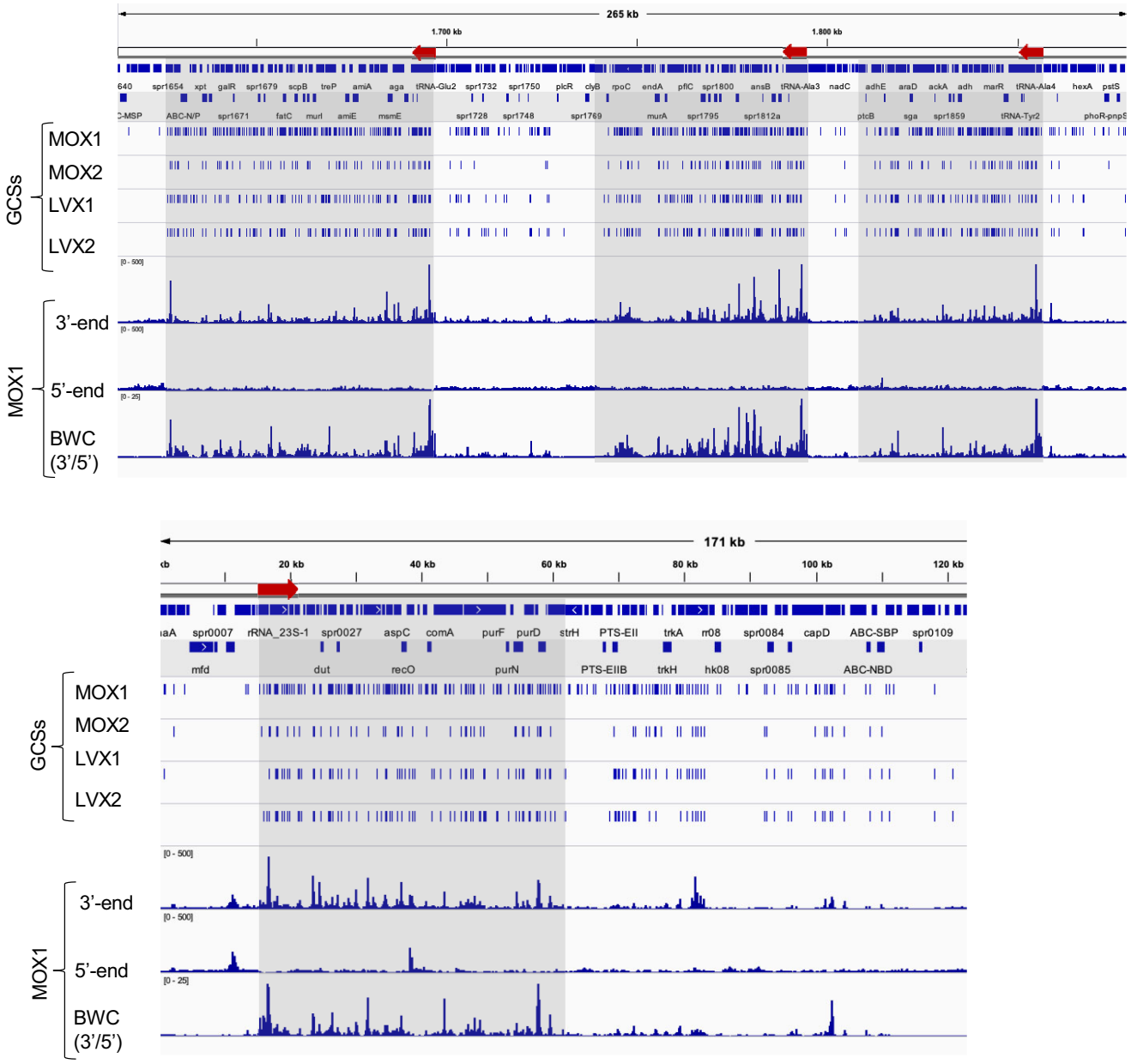

Figure 4. Locations of GCSs near rRNA operons. Red arrows indicate rRNA operons. Areas shadowed in gray indicate the downstream rRNA areas where the GCSs are concentrated. BWC, BigWigCompare.

discrepancies between the LVX and MOX treatments could be attributed to Topo IV being cleaved at different sequences than those recognized by gyrase, as has been reported for *E. coli* Topo IV [55].

The lower gyrase activity on methylated pLS1 could reflect a lower *in vivo* Sc level, since gyrase and Topo I are responsible for maintaining Sc levels in *S. pneumoniae* [24]. This plasmid, which contains nine GATC sites in its sequence, was obtained from the Dpn-isogenic strains (Fig. 8 A). To test this hypothesis, the pLS1 plasmids obtained from the three Dpn-isogenic strains were subjected to two-dimensional agarose gel electrophoresis (Fig. 9). The Sc density (σ) was greater in the plasmid obtained from the DpnI strain than in the plasmid obtained from the DpnII strain ($P = .003$) and greater than in the plasmid obtained from the DpnIII strain ($P = .047$). Similarly, the Sc density of the plasmid obtained from the DpnII strain was greater than that obtained from the DpnIII strain ($P = .024$). The σ values of the plasmid topoisomers obtained from the DpnI strain differed by ∼11.9% and 6.8%, respectively, from those obtained from the DpnII and DpnIII strains. This finding indicates that the methylated plasmid was more relaxed than the unmethylated plasmid. The difference in Sc observed in the plasmids reflects differences in chromosomal Sc levels [27]. The observed variation in Sc is consistent with the level of relaxation, which is compatible with cell growth [26, 56].

Gyrase cleavage in the presence of MOX was also tested *in vitro* using the plasmid pLS1 as the substrate (Fig. 9B). Greater cleavage was detected in pLS1 obtained from the DpnI strain than in pLS1 obtained from the DpnII or DpnIII strains in the presence of MOX. These results suggest that methylation at GATC affects gyrase cleavage, which is in accordance with

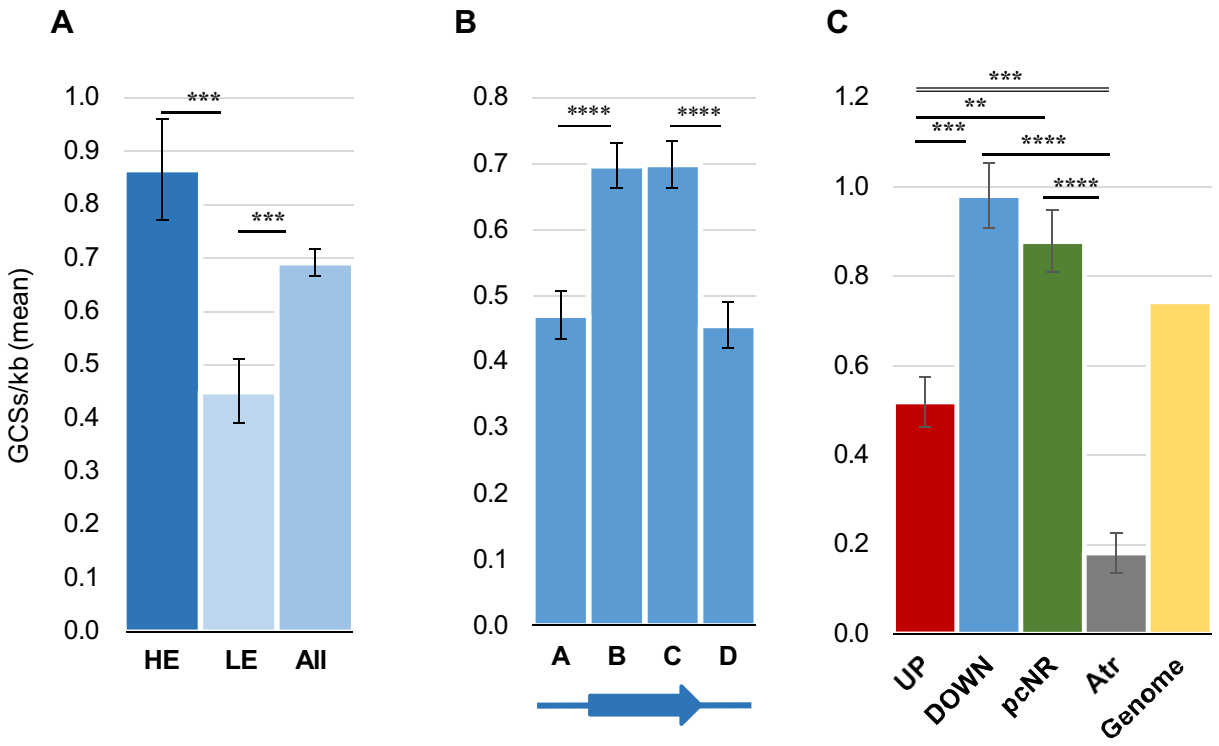

Figure 5. The location of GCSs is related to transcription efficiency. (**A**) Differential location of HE genes versus those with low expression (LEs). (**B**) GCSs are localized preferentially at coding regions. (**C**) GCSs are preferentially located at the DOWN and pcNR domains. Statistical significance Chi-square test, $**P \leq .01$, $***P \leq .001$, $****P \leq .0001$.

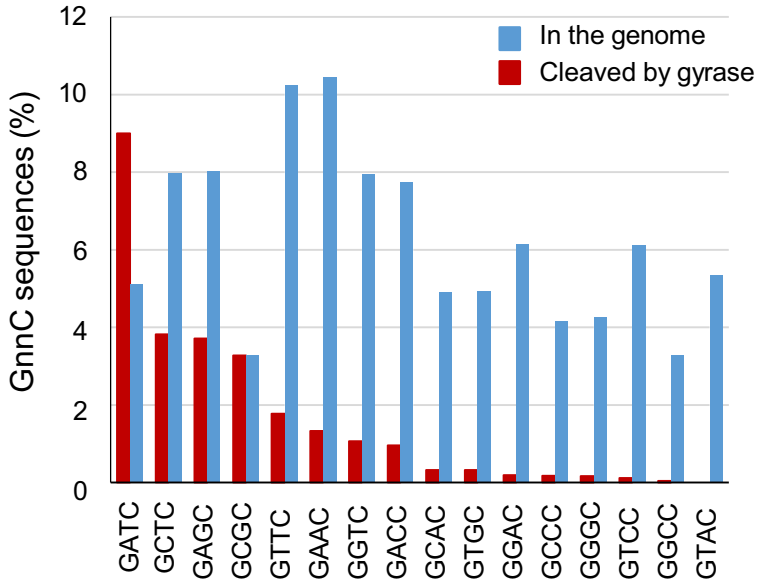

Figure 6. Relationship between the number of GCSs and the 5′-GxxC-3′ sequence in the *S. pneumoniae* R6 genome.

the LVX (gGatCc) and MOX (xGatCx) consensus sequences (Fig. 2D).

The presence of methylation at GATC affects the development of LVX resistance

We demonstrated that gyrase activity is lower on methylated GATC sequences, both *in vitro* and *in vivo* (Figs 8 and 9). Based on these findings, we hypothesized that isolates carrying methylated GATC sequences (DpnII and DpnIII) would be more likely to develop resistance to FQs than nonmethylated isolates (DpnI). We developed LVX resistance as previously described [57, 58]. We cultured three isogenic T1 (R6, ParCS79F) strains, each carrying a different DpnI system (DpnI, DpnII, or DpnIII), for 4 h in the presence of 1 × MIC of LVX. Then, we evaluated the appearance of resistant mutants by plating on several LVX concentrations (Fig. 10A). At 1 × MIC, significantly more resistant cells were detected in the DpnII and DpnIII strains compared to than in the DpnI strain. At 2 × and 4 × MIC, resistant colonies were isolated from

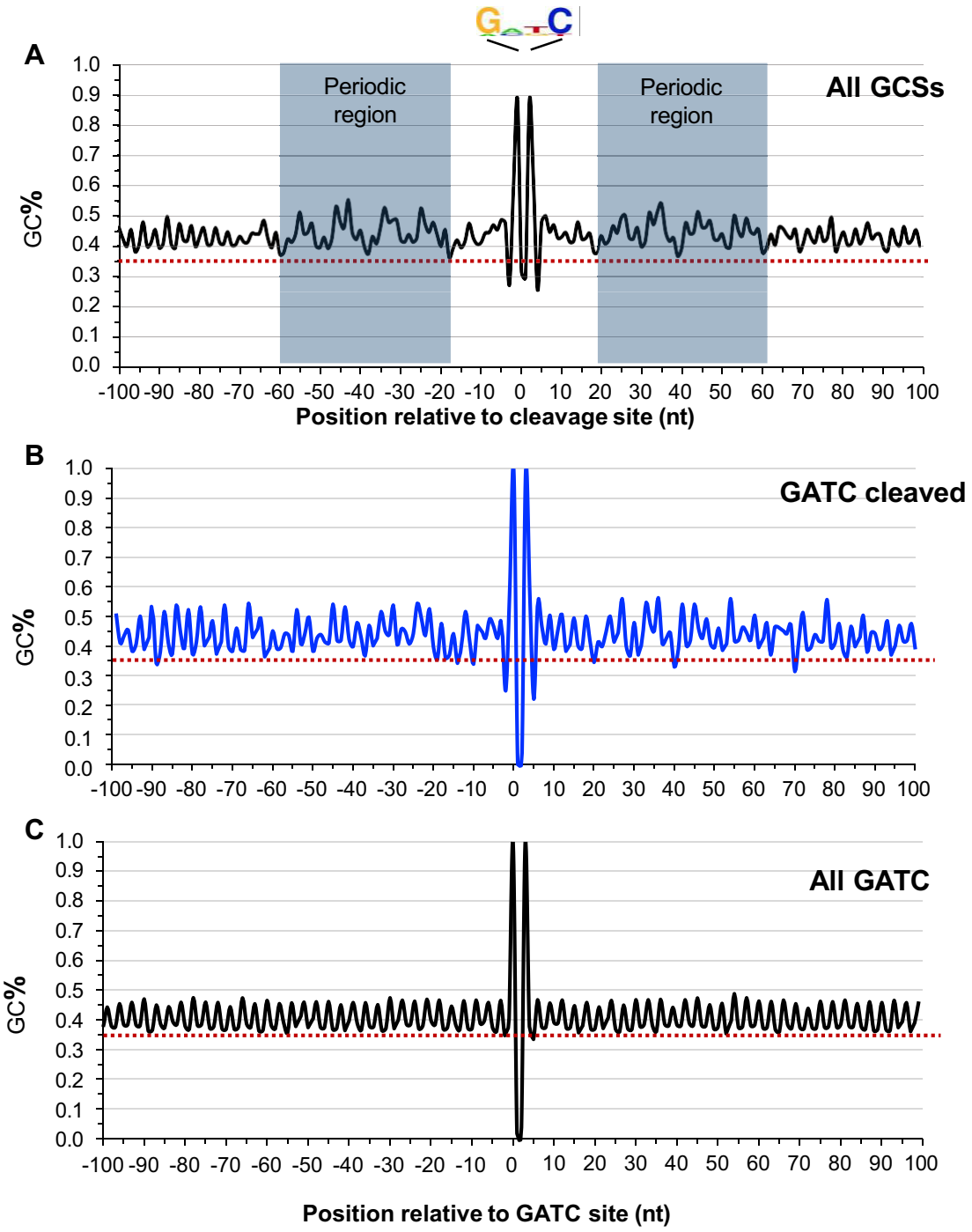

Figure 7. GC content around positions −100 to +100 nt of the GCSs.

the DpnII and DpnIII strains, but not the DpnI strain. These results demonstrate that mutants appear more frequently in strains with GATC methylation. The quinolone resistance-determining regions (QRDRs) of *parC* and *gyrA* from the isolated colonies were sequenced as described previously [9] and are shown in Fig. 10B. The results revealed that the resistant mutants carry the ParCS79F change, which is present in the T1 parental strain, as well as the classical changes associated with FQ resistance [9, 59]: GyrA S81F, S81Y, and E85K. These results are consistent with preferential mutation selection in strains with methylated GATC sites.

Discussion

The number of GCSs estimated in this study, which is common to all FQ treatments tested, was 1517 (Figs 1 and 2), close to the number of sites estimated by the same method for *E. coli* under treatment with the FQs ciprofloxacin and ofloxacin, which was 1921 [42]. These numbers are also close to the number of gyrase enzymes (heterodimer $GyrA_2GyrB_2$) in *S. pneumoniae*, which we estimated to be ∼1092, indicating a 1:1.3 proportion of gyrase and Topo I molecules [24]. The similar number of Topo I and gyrase molecules per cell and the number of GCSs in these bacteria are consistent with the twin

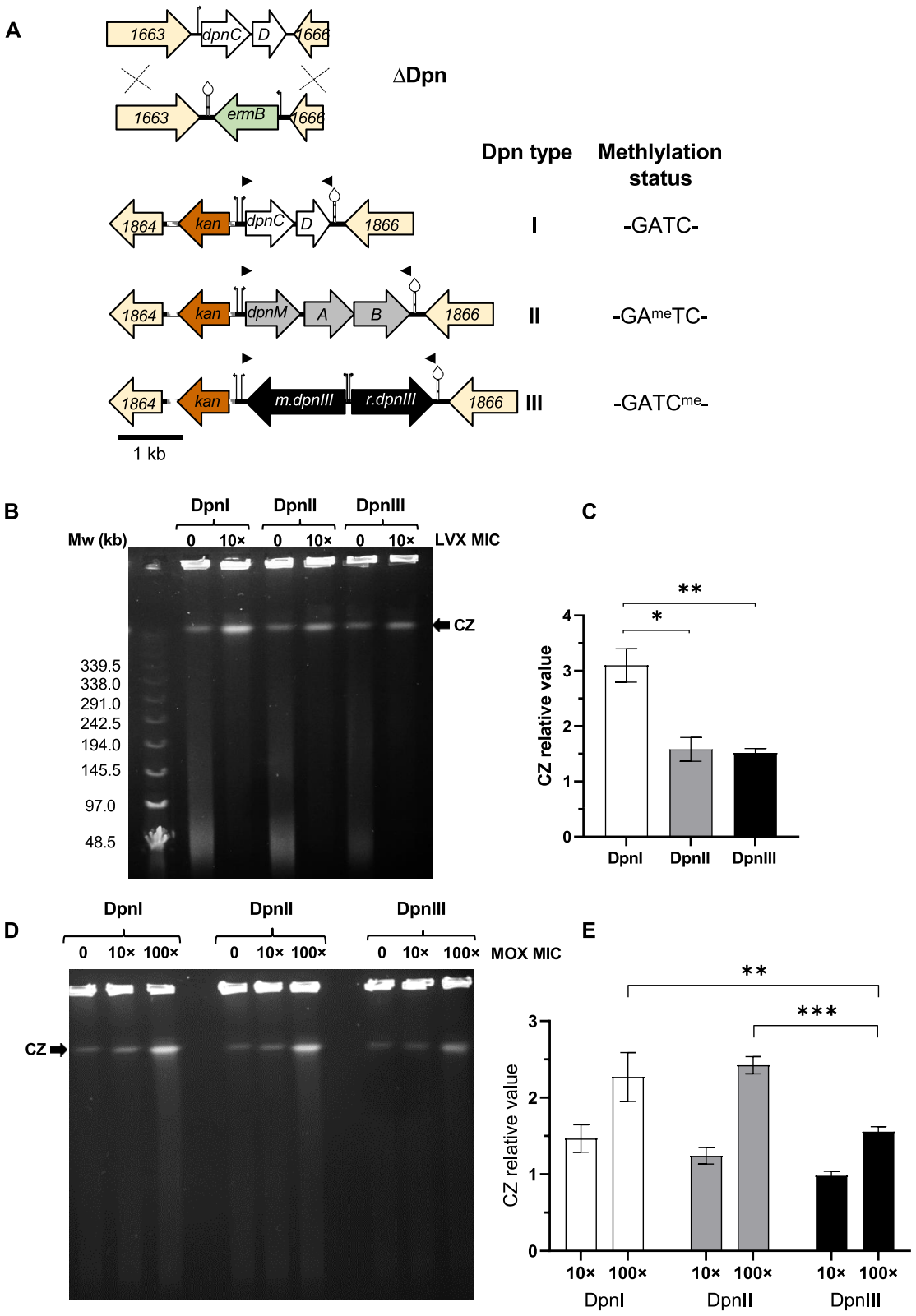

Figure 8. Cleavage by gyrase is inhibited by methylation at GATC. (**A**) Representation of T1 isogenic strains containing the three Dpn systems identified in *S. pneumoniae* at the *spr1865* locus. These strains are derived from T1(R6 ParCS79F)ΔDpn, which was constructed by replacing the DpnI system with *ermB*. The genes are indicated by arrows, and the oligonucleotides used to amplify the *dpn* genes are shown as black arrowheads. Promoters are shown as curved arrows and transcription terminators are shown as stem–loop structures. (**B**) Cleavage in the presence of LVX. PFGE gel of the T1ΔDpn strain carrying either the DpnI (**I**), DpnII (II), or DpnIII (III) system. Cultures grown to OD_{620nm} = 0.4 were treated for 15 min with or without the drug. (**C**) The *Y* axis represents the signal of the CZ divided by the combined signal of the lane plus well, calculated relative to that of untreated cultures. The results are presented as the mean ± SD of three independent replicates. (**D**) Cleavage of cultures grown as indicated in the presence of the indicated MOX concentrations. (**E**) Variations under MOX treatments estimated as in panel (C). The statistical significance was determined via two-way Analysis of variance, with the following thresholds: $**P \leq .01$; $***P \leq .001$.

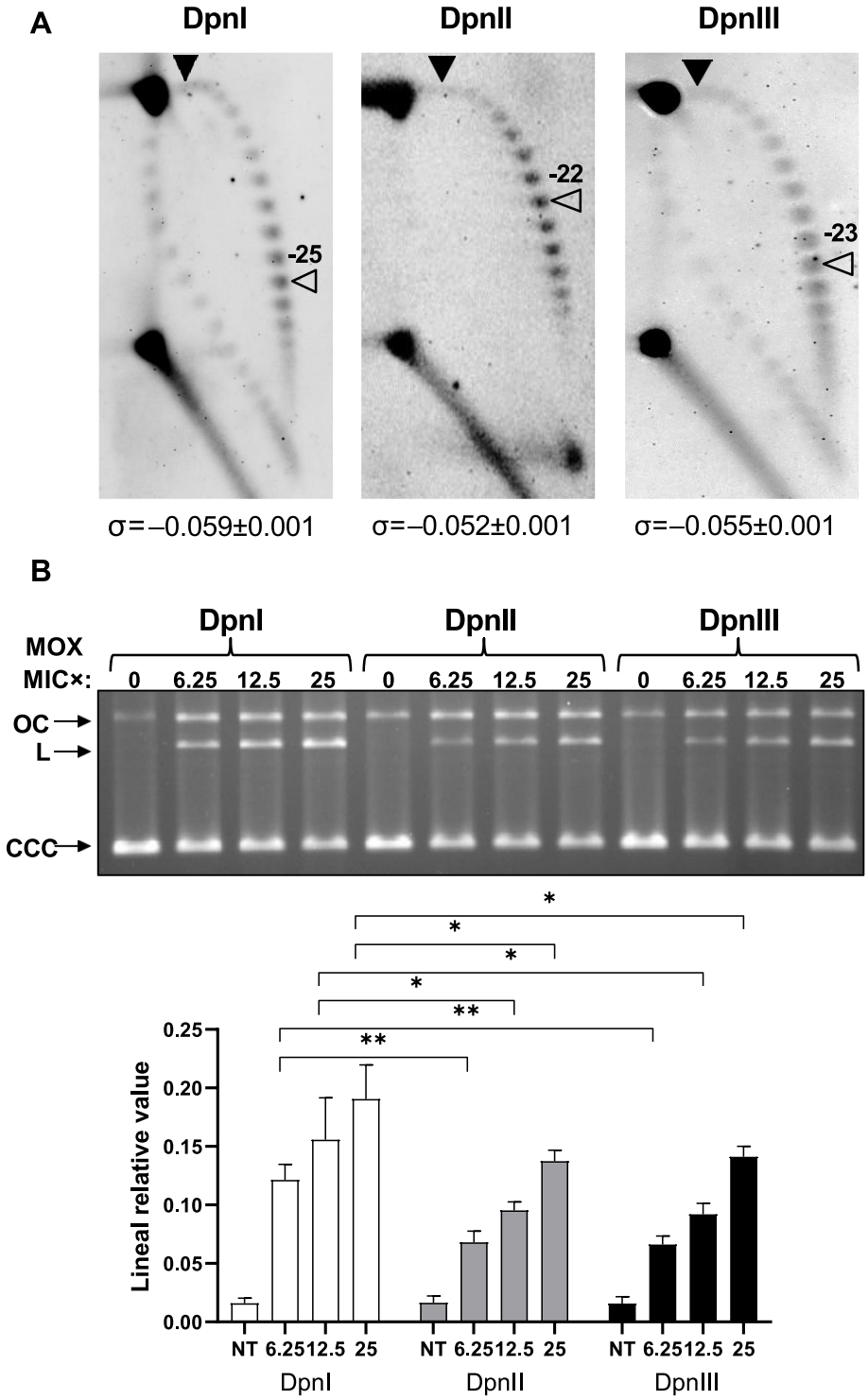

Figure 9. The Sc level is affected by methylation at GATC. (**A**) Two-dimensional gel electrophoresis of pLS1 plasmids obtained from Dpn-isogenic strains. The black arrowhead indicates the topoisomer that migrated with $\Delta Lk = 0$ in the second dimension and has a $\Delta Wr = -14$ (the number of positive supercoils induced by 2 μg/ml chloroquine). The empty arrowhead indicates the most abundant topoisomer. The Sc densities (σ values) were calculated as: Lk of the most abundant topoisomer/Lk_0, where Lk_0 = size of the plasmid/10.5 (number of bp per turn of the double helix). The σ value (mean ± SD, $n = 3$) is indicated. (**B**) *In vitro* cleavage in the presence of MOX and quantification of the activity. The pLS1 plasmid obtained from the indicated Dpn-isogenic strains was incubated with reconstituted gyrase as described in the "Materials and methods" section.The signal of the linear form divided by the whole signal of the plasmid (CCC + L + OC) is shown. The statistical significance was determined via *t*-test, $*P \leq .05$; $**P \leq .01$.

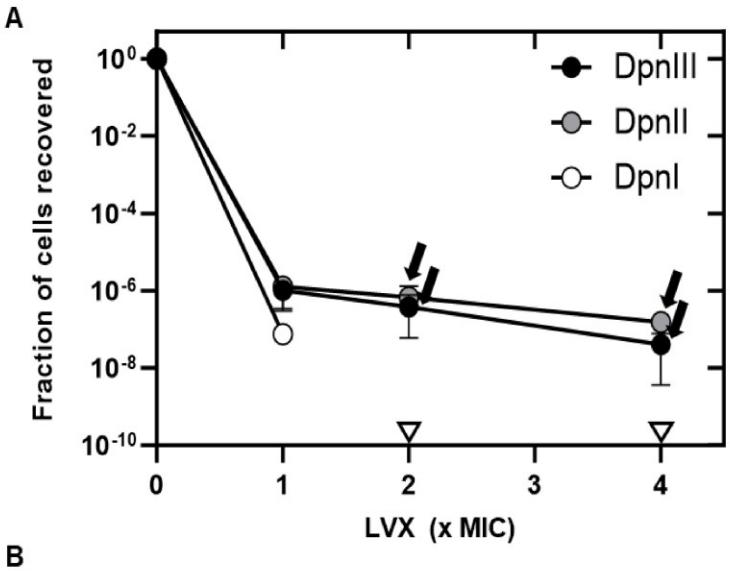

B

Strain	LVX (µg/ml)	N	Sequence	Change
R6			79-GGGGATTCCTCTATTTATGAAGCCATG-87	
T1(DpnII)	4	1	-------A----------	S81Y
	4	1	-------T----------	S81F
	4	2	----------A---------	E85K
T1(DpnIII)	4	1	-------A----------	S81Y
	4	1	-------T----------	S81F
	4	2	----------A---------	E85K
T1(DpnII)	8	3	-------T----------	S81F
T1(DpnIII)	8	3	-------T----------	S81F

Figure 10. Strains with methylated GATC sites are more likely to develop LVX resistance than those with nonmethylated sites. Overnight cultures were grown in A + Y medium until the OD_{620} reached 0.4. Then, the cultures were diluted 20-fold in 500 ml of the same medium and grown until $OD_{620} = 0.4$. LVX was then added to the cultures at a concentration of 1 × MIC, and the cultures were grown for 4 h. The bacteria were recovered by centrifugation, and the cells were suspended at a concentration of 2.5×10^{10} CFU/ml. The cells were plated on A + Y agar plates containing the indicated LVX concentrations. The triangle indicates no colony recovery. (**A**) Recovery of LVX-resistant mutants. The results are presented as the means ± SDs of two independent replicates. (**B**) Point mutations found in the QRDR in *gyrA* of selected isolates.

Sc domain model [32], with the important role of both gyrase and Topo I in transcription [37, 38], and with the interaction of Topo I with RNA polymerase [36–38].

Although the size of the pneumococcal chromosome (~2 Mb) is approximately half of that of the *E. coli* chromosome, the similar number of GCSs observed in both bacteria under FQ treatment suggests that the density of chromosome-bound gyrase is greater in *S. pneumoniae* than in *E. coli*, including those associated with the transcriptional machinery. Gyrase plays a predominant structural role in chromosome compaction in *S. pneumoniae*, a role normally played by nucleoid-associated proteins in *E .coli*. There is a lack of these kind of proteins in *S. pneumoniae*. Their role is played in *S. pneumoniae* by both gyrase and Histone-like protein (HU) [60]. Among the 1 517 GCSs, 1 411 were located between protein-coding genes, mainly in the coding regions of genes in the DOWN and pcNR domains (Fig. 5). The genes in these domains are the most highly transcribed, supporting the essential role of gyrase in transcription. While pcNR genes are not subjected to Sc changes [29], genes in DOWN domains are indeed subjected to Sc status, which are down-regulated under DNA relaxation mediated by gyrase inhibition with novobiocin. The upregulation of UP domain genes in the transcriptomic response to DNA relaxation could be related to their AT content, which is greater than that of DOWN domain genes [26]. DNA relaxation in UP domains would favor transcription, as observed in *E. coli*. In this bacterium, genes induced by relaxation have significantly higher AT contents in both the upstream and coding regions [61]. Accordingly, AT enrichment, both upstream and in the coding regions of upregulated genes induced after relaxation, has also been reported in *E. coli* [61]. However, we do not have an explanation for the coordinated downregulation of genes of DOWN domains under DNA relaxation. The results presented in this study partially explain this effect, which is triggered by novobiocin treatment [26]. Since gyrase preferentially facilitates the transcription of genes in DOWN domains, the increased GCSs on these domains would be responsible for the preferential inhibition of transcription of these genes. On the other hand, genes in ATr domains, which exhibit the lowest transcription among the genes in the genome also have the lowest number of GCSs.

In relation to GCSs not associated with protein-coding genes, the relationship of gyrase with the removal of positive Sc downstream RNA polymerase was evident when the GCSs were analyzed in proximity to the four rRNA operons (Fig. 4). These genes are the most highly transcribed genes.

The same four-base GCS motif was identified regardless of the FQ used (Fig. 2). However, slight differences were found between LVX and MOX when a consensus sequence with six bases was considered. The LVX consensus sequence was gGatCc, whereas the MOX consensus sequence was xGatCx (Fig. 2D). These results suggest that the identified sequences may not fully reflect the genomic position of gyrase in the absence of FQs. GATC was the most frequently cut sequence by gyrase accounting for 21.2% of all GCSs. Although GATC is not the most frequent GxxC sequence in the genome, it is indeed the most frequently cleaved sequence by gyrase (Fig. 6), which supports the specificity of the GCSs determined in this study. This motif is similar to that reported for *E. coli* gyrase under FQ treatment [42], although not identical, supporting the different susceptibilities of these gyrase enzymes to FQs. The symmetrical pattern with phased 10-bp GC content observed on both sides of the GATC cleaved sites would indicate that the bending ability of the DNA could contribute to gyrase binding, as suggested for *E. coli* [42]. This GATC sequence is the recognition site of the DpnII and DpnIII methylases of *S. pneumoniae*.

The results of this study could partially explain our previous epidemiological studies of *S. pneumoniae* FQ resistance in Spain. These studies revealed that the frequency of FQ resistance stabilized at ∼2.5% in the three periods analyzed: 2002 [62], 2006 [9], and 2012 [59]. One of the factors contributing to this stabilization was the change in the distribution of prevalent genotypes because of the implementation of vaccines. In fact, in 2002 the most prevalent genotype was Spain^{23F}-ST81, which almost disappeared in 2006 and 2012 because of the implementation of PCV7 and PCV13 vaccines, which include capsule 23F. The most prevalent genotypes in 2006 and 2012 were Spain^{9V}-ST156 and Sweden^{15A}-ST63, respectively. These clones remained since they underwent capsule interchanges to adapt to the new vaccines. Interestingly, among these three more prevalent FQ-resistant genotypes, two have methylated GATC sequences: Spain^{23F}-ST81 (DpnIII system) and Sweden^{15A}-ST63 (DpnII system). These data suggest that methylation at either A (DpnII) or G (DpnIII) in the GATC motif modifies both gyrase activity and Sc (Fig. 9) and gyrase cleavage, as shown by our PFGE analysis (Fig. 8). While DpnIII is exclusive to the Spain^{23F}-ST81 genotype, there is no information about the frequency of DpnI and DpnII in the *S. pneumoniae* population. As an approach to estimate this frequency, a BLASTP analysis of the nonredundant *S. pneumoniae* sequences at NCBI, by using either the DpnI protein DpnC (POA460) or the DpnII protein DpnM (PO4043) with a 100% identity filter, returns 109 and 50 hits, respectively. Even when DpnI strains are more common in the database, they are not more common among FQ-resistant isolates. This finding suggests that the DpnII and DpnIII strains that methylate GATC are more resistant to subinhibitory concentrations of FQs, since gyrase cleavage is lower on methylated sequences; this would favor the emergence of resistance in the DpnII and DpnIII isolates related to DpnI (Fig. 10), resulting in a stabilization of resistance levels. In this way, the complementary in specificity and mutually exclusive DpnI and DpnII systems [63] enable cells to resist bacteriophage attack [64] and also play a role in FQ resistance. The genetic basis of the phenotypic variation in these restriction systems in *S. pneumoniae* depends on a cassette mechanism, in which alternative gene clusters are positioned at a specific location in the chromosome [65]. This alternation could also play a role in the evolution of FQ resistance. More epidemiological studies are necessary to understand this effect.

The GATC methylome is relevant for *S. pneumoniae* survival under FQ stress. Similarly, a lack of adenine methylation at GATC in *E. coli* has been reported to potentiate FQ activity. Methyl-dependent mismatch repair is deleterious and, fueled by the drug-induced error-prone activity of the polymerase Pol IV, overwhelms cells with toxic DNA breaks [66]. In *S. pneumoniae*, which lacks the signaling of the mismatch repair system by GATC methylation [67], the deleterious effect of a nonmethylated GATC would be caused by increased fragmentation mediated by gyrase, as indicated by our results. These data make DNA methylation an attractive target for modulating the activity of FQs.

Acknowledgements

Author contributions: Conceptualization: Maria-José Ferrándiz, Pablo Hernández, and Adela G. de la Campa. Data curation: Pablo Hernández. Formal analysis: Pablo Hernández and Adela G. de la Campa. Funding acquisition: Adela G. de la Campa. Investigation: Maria-José Ferrándiz. Methodology: Maria-José Ferrándiz, Pablo Hernández, and Adela G. de la Campa. Project administration: Adela G. de la Campa. Resources: Maria-José Ferrándiz, Pablo Hernández, and Adela G. de la Campa. Software: Pablo Hernández. Validation: Maria-José Ferrándiz and Adela G. de la Campa. Visualization: Pablo Hernández and Adela G. de la Campa. Writing—original draft: Pablo Hernández and Adela G. de la Campa. Writing—review and editing: Maria-José Ferrándiz, Pablo Hernández, and Adela G. de la Campa.

Supplementary data

Supplementary data is available at NAR Online.

Conflict of interest

None declared.

Funding

MICIN/AEI/10.13039/501100011033/FEDER, UE [PID2024-157350OB-I00, PID2021-124738OB-100]. Funding to pay the Open Access publication charges for this article was provided by projects PID2021-124738OB-100 to A.G.C. and PID2024-157350OB-I00 to M.J.F. and A.G.C., financed by MICIN/AEI/10.13039/501100011033/FEDER, UE.

Data availability

The ChIP-seq data have been deposited in the NCBI Short Read Archive (SRA) database with the BioProject PRJNA1218523.

References

1. World Health Organization. Pneumococcal conjugate vaccine for chilhood immunization-WHO position paper. *Wkly Epidemiol Rec* 2007;82:93–104.
2. Jacobs MR, Felmingham D, Appelbaum PC *et al.* and the Alexandre Project Group. The Alexander project 1998–200: susceptibility of pathogens isolated from community-acquired

respiratory tract infection to commomnly used antimicrobial agents. *J Antimicrob Chemother* 2003;52:229–46. https://doi.org/10.1093/jac/dkg321
3. Metlay JP, Waterer GW, Long AC *et al.* Diagnosis and treatment of adults with community-acquired pneumonia. An official clinical practice guideline of the American Thoracic Society and Infectious Diseases Society of America. *Am J Respir Crit Care Med* 2019;200:e45–67. https://doi.org/10.1164/rccm.201908-1581ST
4. Junier I, Ghobadpour E, Espeli O *et al.* DNA supercoiling in bacteria: state of play and challenges from a viewpoint of physics based modeling. *Front Microbiol* 2023;14:1192831. https://doi.org/10.3389/fmicb.2023.1192831
5. Muñoz R, de la Campa AG. ParC subunit of DNA topoisomerase IV of *Streptococcus pneumoniae* is a primary target of fluoroquinolones and cooperates with DNA gyrase A subunit in forming resistance phenotype. *Antimicrob Agents Chemother* 1996;40:2252–7. https://doi.org/10.1128/AAC.40.10.2252
6. Janoir C, Zeller V, Kitzis M-D *et al.* High-level fluoroquinolone resistance in *Streptococcus pneumoniae* requires mutations in *parC* and *gyrA*. *Antimicrob Agents Chemother* 1996;40:2760–4. https://doi.org/10.1128/AAC.40.12.2760
7. Pan X-S, Ambler J, Mehtar S *et al.* Involvement of topoisomerase IV and DNA gyrase as ciprofloxacin targets in *Streptococcus pneumoniae*. *Antimicrob Agents Chemother* 1996;40:2321–6. https://doi.org/10.1128/AAC.40.10.2321
8. Fernández-Moreira E, Balas D, González I *et al.* Fluoroquinolones inhibit preferentially *Streptococcus pneumoniae* DNA topoisomerase IV than DNA gyrase native proteins. *Microb Drug Resist* 2000;6:259–67. https://doi.org/10.1089/mdr.2000.6.259
9. de la Campa AG, Ardanuy C, Balsalobre L *et al.* Changes in fluoroquinolone-resistant *Streptococcus pneumoniae* after 7-valent conjugate vaccination, Spain. *Emerg Infect Dis* 2009;15:905–11. https://doi.org/ 10.3201/eid1506.080684
10. Balsalobre L, Ferrándiz MJ, Liñares J *et al.* Viridans group streptococci are donors in horizontal transfer of topoisomerase IV genes to *Streptococcus pneumoniae*. *Antimicrob Agents Chemother* 2003;47:2072–81. https://doi.org/10.1128/AAC.47.7.2072-2081.2003
11. Ardanuy C, de la Campa AG, García E *et al.* Spread of *Streptococcus pneumoniae* serotype 8-ST63 multidrug-resistant recombinant Clone, Spain. *Emerg Infect Dis* 2014;20:1848–56. https://doi.org/ https://doi.org/10.3201/eid2011.131215
12. Drlica K, Malik M, Kerns RJ *et al.* Quinolone-mediated bacterial death. *Antimicrob Agents Chemother* 2008;52:385–92. https://doi.org/10.1128/AAC.01617-06
13. Wang X, Zhao X, Malik M *et al.* Contribution of reactive oxygen species to pathways of quinolone-mediated bacterial cell death. *J Antimicrob Chemother* 2010;65:520–4. https://doi.org/10.1093/jac/dkp486
14. Ferrándiz MJ, Martín-Galiano AJ, Arnanz C *et al.* Reactive oxygen species contribute to the bactericidal effects of the fluoroquinolone moxifloxacin in *Streptococcus pneumoniae*. *Antimicrob Agents Chemother* 2016;60:409–17. https://doi.org/10.1128/AAC.02299-15
15. Brito L, Wilton J, Ferrándiz MJ *et al.* Absence of tmRNA has a protective effect against fluoroquinolones in *Streptococcus pneumoniae*. *Front Microbiol* 2016;7:2164. https://doi.org/10.3389/fmicb.2016.02164
16. García M, Valenzuela M, Ferrándiz M *et al.* Reactive oxygen species production is a major factor directing the postantibiotic effect of fluoroquinolones in *Streptococcus pneumoniae*. *Antimicrob Agents Chemother* 2019;63:e00737–00719. https://doi.org/10.1128/AAC.00737-19
17. Ferrándiz MJ, de la Campa AG. The fluoroquinolone levofloxacin triggers the transcriptional activation of iron transport genes that contribute to cell death in *Streptococcus pneumoniae*. *Antimicrob Agents Chemother* 2014;58:247–57. https://doi.org/10.1128/AAC.01706-13
18. Dwyer DJ, Belenky PA, Yang JH *et al.* Antibiotics induce redox-related physiological alterations as part of their lethality. *Proc Natl Acad Sci USA* 2014;111:2100–9. https://doi.org/10.1073/pnas.1401876111
19. DiNardo S, Voelkel KA, Sternglanz R *et al.* *Escherichia coli* DNA topoisomerase I mutants have compensatory mutations in DNA gyrase genes. *Cell* 1982;31:43–51. https://doi.org/10.1016/0092-8674(82)90403-2
20. Pruss GJ, Manes SH, Drlica K. *Escherichia coli* DNA topoisomerase I mutants: increased supercoiling is corrected by mutations near gyrase genes. *Cell* 1982;31:35–42. https://doi.org/10.1016/0092-8674(82)90402-0
21. Tse-Dinh Y-C. Regulation of the *Escherichia coli* DNA topoisomerase I gene by DNA supercoiling. *Nucl Acids Res* 1985;13:4751–63. https://doi.org/10.1093/nar/13.13.4751
22. Menzel R, Gellert M. Regulation of the genes for *E. coli* DNA gyrase: homeostatic control of DNA supercoiling. *Cell* 1983;34:105–13. https://doi.org/10.1016/0092-8674(83)90140-X
23. Menzel R, Gellert M. Modulation of transcription by DNA supercoiling: a deletion analysis of the *Escherichia coli gyrA* and *gyrB* promoters. *Proc Natl Acad Sci USA* 1987;84:4185–9. https://doi.org/10.1073/pnas.84.12.4185
24. García-López M, Megias D, Ferrándiz MJ *et al.* The balance between gyrase and topoisomerase I activities determines levels of supercoiling, nucleoid compaction, and viability in bacteria. *Front Microbiol* 2023;13:1094692. https://doi.org/10.3389/fmicb.2022.1094692
25. Ferrándiz MJ, Arnanz C, Martín-Galiano AJ *et al.* Role of global and local topology in the regulation of gene expression in *Streptococcus pneumoniae*. *PLoS One* 2014;9:e101574. https://doi.org/10.1371/journal.pone.0101574
26. Ferrándiz MJ, Martín-Galiano AJ, Schvartzman JB *et al.* The genome of *Streptococcus pneumoniae* is organized in topology-reacting gene clusters. *Nucleic Acids Research* 2010;38:3570–81. https://doi.org/10.1093/nar/gkq106
27. García-López M, Hernández P, Megias D *et al.* Physiologic and transcriptomic effects triggered by overexpression of wild type and mutant DNA topoisomerase I in *Streptococcus pneumoniae*. *Int J Mol Sci* 2023;24:15800. https://doi.org/10.3390/ijms242115800
28. Ferrándiz MJ, Martín-Galiano AJ, Arnanz C *et al.* An increase in negative supercoiling in bacteria reveals topology-reacting gene clusters and a homeostatic response mediated by the DNA topoisomerase I gene. *Nucleic Acids Res* 2016;44:7292–303. https://doi.org/10.1093/nar/gkw602
29. Martín-Galiano AJ, Ferrándiz MJ, de la Campa AG. Bridging chromosomal architecture and pathophysiology of *Streptococcus pneumoniae*. *Genome Biol Evol* 2017;9:350–61. https://doi.org/10.1093/gbe/evw299
30. de la Campa AG, Ferrándiz MJ, Martín-Galiano AJ *et al.* The transcriptome of *Streptococcus pneumoniae* induced by local and global changes in supercoiling. *Front Microbiol* 2017;8:1447. https://doi.org/10.3389/fmicb.2017.01447
31. Pruss GJ, Drlica K. Topoisomerase I mutants: the gene on pBR322 that encodes resistance to tetracycline affects plasmid DNA supercoiling. *Proc Natl Acad Sci USA* 1986;83:8952–6. https://doi.org/10.1073/pnas.83.23.8952
32. Liu LF, Wang JC. Supercoiling of the DNA template during transcription. *Proc Natl Acad Sci USA* 1987;84:7024–7. https://doi.org/ 10.1073/pnas.84.20.7024
33. Phoenix PR, M. A, Masse E *et al.* Roles of DNA topoisomerases in the regulation of R-loop formation *in vitro*. *J Biol Chem* 1997;272:1473–9. https://doi.org/ 10.1074/jbc.272.3.1473
34. Masse EP, Phoenix P, Drolet M. DNA topoisomerases regulate R-loop formation during transcription of the *rrnb* operon in *Escherichia coli*. *J Biol Chem* 1997;272:12816–23. https://doi.org/ 10.1074/jbc.272.19.12816
35. Drolet M, Bi X, Liu LF. Hypernegative supercoiling of the DNA template during transcription elongation *in vitro*. *J Biol Chem* 1994;269:2068–74. https://doi.org/10.1016/S0021-9258(17)42136-3
36. Cheng BZ, C. X, Ji C *et al.* Direct interaction between *Escherichia coli* RNA polymerase and the zinc ribbon domains of DNA

topoisomerase I. *J Biol Chem* 2003;278:30705–10. https://doi.org/10.1074/jbc.M303403200
37. Ferrándiz MJ, Hernández P, de la Campa AG. Genome-wide proximity between RNA polymerase and DNA topoisomerase I supports transcription in *Streptococcus pneumoniae*. *PLoS Genet* 2021;17:e1009542. https://doi.org/10.1371/journal.pgen.1009542
38. Ahmed W, Sala C, Hegde SR *et al.* Transcription facilitated genome-wide recruitment of topoisomerase I and DNA gyrase. *PLoS Genet* 2017;13:e1006754. https://doi.org/10.1371/journal.pgen.1006754
39. Sutormin D, Galivondzhyan A, Musharova O *et al.* Interaction between transcribing RNA polymerase and topoisomerase I prevents R-loop formation in *E. coli*. *Nat Commun* 2022;13:4524. https://doi.org/10.1038/s41467-022-32106-5
40. Leo E, Gould KA, Pan XS *et al.* Novel symmetric and asymmetric DNA scission determinants for *Streptococcus pneumoniae* topoisomerase IV and gyrase are clustered at the DNA breakage site. *J Biol Chem* 2005;280:14252–63. https://doi.org/10.1074/jbc.M500156200
41. Arnoldi E, Pan XS, Fisher LM. Functional determinants of gate-DNA selection and cleavage by bacterial type II topoisomerases. *Nucl Acids Res* 2013;41:9411–23. https://doi.org/10.1093/nar/gkt696
42. Sutormin D, Rubanova N, Logacheva M *et al.* Single-nucleotide-resolution mapping of DNA gyrase cleavage sites across the *Escherichia coli* genome. *Nucl Acids Res* 2019;47:1601. https://doi.org/10.1093/nar/gky1312
43. Balsalobre L, de la Campa AG. Fitness of *Streptococcus pneumoniae* fluoroquinolone-resistant strains with topoisomerase IV recombinant genes. *Antimicrob Agents Chemother* 2008;52:822–30. https://doi.org/10.1128/AAC.00731-07
44. Lacks SA, López P, Greenberg B *et al.* Identification and analysis of genes for tetracycline resistance and replication functions in the broad-host-range plasmid pLS1. *J Mol Biol* 1986;192:753–65. https://doi.org/10.1016/0022-2836(86)90026-4
45. Lacks SA, Springhorn SS. Transfer of recombinant plasmids containing the gene for DpnII DNA methylase into strains of *Streptococcus pneumoniae* that produce DpnI or DpnII restriction endonucleases. *J Bacteriol* 1984;158:905–9. https://doi.org/10.1128/jb.158.3.905-909.1984
46. Eutsey RA, Powell E, Dordel J *et al.* Genetic stabilization of the drug-resistant PMEN1 pneumococcus lineage by its distinctive DpnIII restriction-modification system. *mBio* 2015;6:e00173. https://doi.org/10.1128/mBio.00173-15
47. Balsalobre L, Ferrándiz MJ, de Alba G *et al.* Nonoptimal DNA topoisomerases allow maintenance of supercoiling levels and improve fitness of *Streptococcus pneumoniae*. *Antimicrob Agents Chemother* 2011;55:1097–105. https://doi.org/10.1128/AAC.00783-10
48. Martín-Parras L, Lucas I, Martínez-Robles ML *et al.* Topological complexity of different populations of pBR322 as visualized by two-dimensional agarose gel electrophoresis. *Nucleic Acids Research* 1998;26:3424–32. https://doi.org/10.1093/nar/26.14.3424
49. Afgan E, Baker D, Batut B *et al.* The Galaxy platform for accessible, reproducible and collaborative biomedical analyses: 2018 update. *Nucl Acids Res* 2018;46:W537–44. https://doi.org/10.1093/nar/gky379
50. Grant JR, Enns E, Marinier E *et al.* Proksee: in-depth characterization and visualization of bacterial genomes. *Nucl Acids Res* 2023;51:W484–92. https://doi.org/10.1093/nar/gkad326
51. Lacks S, Greenberg B. A deoxyribonuclease of *Diplococcus pneumoniae* specific for methylated DNA. *Journal of Biological Chemistry* 1975;250:4060–6. https://doi.org/10.1016/S0021-9258(19)41386-0
52. de la Campa AG, Kale P, Springhorn SS *et al.* Proteins encoded by the DpnII restriction gene cassette. Two methylases and an endonuclease. *J Mol Biol* 1987;196:457–69. https://doi.org/10.1016/0022-2836(87)90024-6
53. Cerritelli S, Springhorn SS, Lacks SA. DpnA, a methylase for single-strand DNA in the Dpn II restriction system, and its biological function. *Proc Natl Acad Sci USA* 1989;86:9223–7. https://doi.org/10.1073/pnas.86.23.9223
54. Lacks SA, Ayalew S, de la Campa AG *et al.* Regulation of competence for genetic transformation in *Streptococcus pneumoniae*: expression of *dpnA*, a late competence gene encoding a DNA methyltransferase of the DpnII restriction system. *Mol Microbiol* 2000;35:1089–98. https://doi.org/10.1046/j.1365-2958.2000.01777.x
55. Sutormin D, Galivondzhyan A, Gafurov A *et al.* Single-nucleotide resolution detection of Topo IV cleavage activity in the *Escherichia coli* genome with Topo-Seq. *Front Microbiol* 2023;14:1160736. https://doi.org/10.3389/fmicb.2023.1160736
56. Drlica K. Control of bacterial DNA supercoiling. *Mol Microbiol* 1992;6:425–33. https://doi.org/10.1111/j.1365-2958.1992.tb01486.x
57. López E, Domenech A, Ferrándiz MJ *et al.* Induction of prophages by fluoroquinolones in *Streptococcus pneumoniae*: implications for emergence of resistance in genetically-related clones. *PLoS One* 2014;9:e94358. https://doi.org/10.1371/journal.pone.0094358
58. Li X, Zhao X, Drlica K. Selection of *Streptococcus pneumoniae* mutants having reduced susceptibility to moxifloxacin and levofloxacin. *Antimicrob Agents Chemother* 2002;46:522–4. https://doi.org/10.1128/AAC.46.2.522-524.2002
59. Domenech A, Tirado-Vélez JM, Fenoll A *et al.* Fluoroquinolone-resistant pneumococci: dynamics of serotypes and clones in Spain in 2012 compared with those from 2002 and 2006. *Antimicrob Agents Chemother* 2014;58:2393–9. https://doi.org/10.1128/AAC.02669-13
60. Ferrándiz MJ, Carreño D, Ayora S *et al.* HU of *Streptococcus pneumoniae* is essential for the preservation of DNA supercoiling. *Front Microbiol* 2018;9:493. https://doi.org/10.3389/fmicb.2018.00493
61. Peter BJ, Arsuaga J, Breier AM *et al.* Genomic transcriptional response to loss of chromosomal supercoiling in *Escherichia coli*. *Genome Biol* 2004;5:R87. https://doi.org/10.1186/gb-2004-5-11-r87
62. de la Campa AG, Balsalobre L, Ardanuy C *et al.* Fluoroquinolone resistance in penicillin-resistant *Streptococcus pneumoniae* clones, Spain. *Emerg Infect Dis* 2004;10:1751–9. https://doi.org/10.3201/eid1010.040382
63. Lacks S, Greenberg B. Complementary specificity of restriction endonucleases of *Diplococcus pneumoniae* with respect to DNA methylation. *J Mol Biol* 1977;114:153–68. https://doi.org/10.1016/0022-2836(77)90289-3
64. Muckerman CC, Springhorn SS, Greenberg B *et al.* Transformation of restriction endonuclease phenotype in *Streptococcus pneumoniae*. *J Bacteriol* 1982;152:183–90. https://doi.org/10.1128/jb.152.1.183-190.1982
65. Lacks SA, Mannarelli BM, Springhorn SS *et al.* Genetic basis of the complementary DpnI and DpnII restriction systems of *S. pneumoniae*: an intercellular cassette mechanism. *Cell* 1986;46:993–1000. https://doi.org/10.1016/0092-8674(86)90698-7
66. Cohen NR, Ross CA, Jain S *et al.* A role for the bacterial GATC methylome in antibiotic stress survival. *Nat Genet* 2016;48:581–6. https://doi.org/10.1038/ng.3530
67. Lacks SA, Dunn JJ, Greenberg B. Identification of base mismatches recognized by the heteroduplex-DNA-repair system of *Streptococcus pneumoniae*. *Cell* 1982;31:327–36. https://doi.org/10.1016/0092-8674(82)90126-X

Received: February 3, 2025. **Revised:** October 9, 2025. **Accepted:** October 11, 2025